2007 IEEE International Conference on
Robotics and Automation
Roma, Italy, 10-14 April 2007

Nonlinear Image Based Visual Servoing Using Parallel Robots

Zhen Qi and John E. McInroy

Abstract— **This paper considers the control problem of an eye-in-hand type of parallel robot based precision pointing system (PRBPPS) in which the visual sensor is mounted on the platform of the parallel robot. The aim of the control is to move the platform of the parallel robot such that the image feature points reach the desired locations. An adaptive supervisory fuzzy logic controller (ASFLC) is first designed to compensate for the uncertainties of the parallel robot and uncertainty of the image Jacobian, then a hybrid controller (HC) including the image-based nonlinear controller (IBNC) and the ASFLC is derived by using the Lyapunov direct method to realize the precision position regulation (PPR). The stability of the closed-loop system in the Lyapunov sense is proven theoretically. The simulation results demonstrate that the PRBPPS realizes PPR with very good robustness to parameter uncertainties.**

I. Introduction

Precision Pointing has wide applications in aerospace and military fields (such as ground vehicles (GVs)). The control of precision pointing systems (PPS) is the fusion of image processing, dynamics, and control theory. Position-Based Visual Servo (PBVS) and Image Based Visual Servo (IBVS) are two commonly used methods. The PBVS has drawbacks such as requirement of the accurate 3D model of the target, sensitivity to camera calibration errors, poor robustness of pose estimation [1], and no control performed in the image [2]. One of the chief advantages to IBVS over PBVS is that the positioning accuracy of the system is less sensitive to camera calibration errors [3]. Thus IBVS is considered in this paper. For the PPS, especially those used in GVs which move in rough terrain, the external disturbance will limit the ability of the image processing software and potentially cause the target to move out of the camera field of view. So disturbance rejection and vibration isolation should be considered in order to improve the pointing performance of the PPS.

Parallel robots consist of a set of actuators arranged in a closed kinematic chain. The parallel arrangement of actuators provides an excellent force-to-weight ratio, and improved accuracy by reducing aggregate joint measurement errors. This makes the Parallel Robot well suited for precision applications, and much research work has been done during the last few years. McInroy *et al.* [4], [5], [6] developed techniques for fault tolerant precision hexapod pointing. Studies in [7],[8] also investigated the use of Parallel Robots for vibration isolation. Because much research has been done on disturbance rejection using parallel robots in [4]-[8], we do not consider this problem here, and assume that the external disturbance is rejected by using proper control techniques. The main concern of this paper is the set-point regulation of the PPS with uncertainties caused by the dynamics of parallel robots and the object depth measurements in the environment with static objects.

Zhen Qi is with the Department of Electrical and Computer Engineering, University of Wyoming, Laramie WY 82070, USA swamqi@uwyo.edu
John E. McInroy is with Faculty of the Department of Electrical and Computer Engineering, University of Wyoming, Laramie WY 82070, USA mcinroy@uwyo.edu

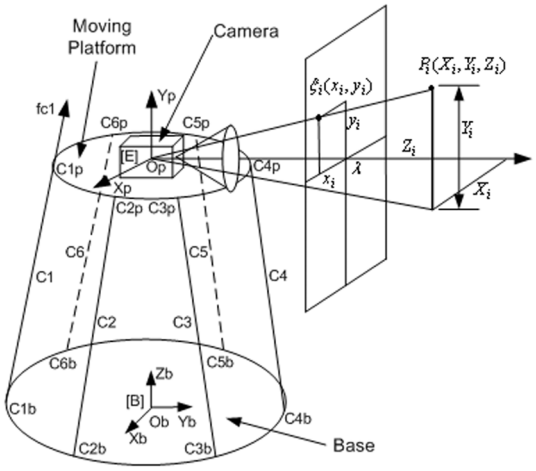

Fig. 1. The sketch of the PRBPPS.

II. Parallel Robot Based Precision Pointing Systems (PRBPPS)

As shown in Fig. (1), the PRBPPS is made up of a parallel robot and a camera which is mounted on the platform of the parallel robot. The mathematical description of the PRBPPS consists of the dynamics of the parallel robot and the camera model.

Because of the presence of structured and unstructured uncertainties, the exact dynamic model of the parallel robot will never be known. If the modeling errors caused by the uncertainties are bounded with known functions, we can get the real dynamics by combining the estimated dynamics with the modeling errors.

The estimated dynamics of the parallel robot is following [14]:

$$\bar{\mathbf{D}}(\boldsymbol{\chi})\ddot{\boldsymbol{\chi}} + \bar{\mathbf{C}}(\boldsymbol{\chi},\dot{\boldsymbol{\chi}})\dot{\boldsymbol{\chi}} + \bar{\mathbf{G}}(\boldsymbol{\chi}) = \bar{\boldsymbol{\tau}}, \tag{1}$$

where $\bar{\mathbf{D}}(\boldsymbol{\chi}) = \begin{bmatrix} m\mathbf{I}'_{3\times3} & \mathbf{0}_{3\times3} \\ \mathbf{0}_{3\times1} & \mathbf{I}'_{3\times3} \end{bmatrix}$, $\bar{\mathbf{C}}(\boldsymbol{\chi},\dot{\boldsymbol{\chi}})\dot{\boldsymbol{\chi}} = \begin{bmatrix} \mathbf{0}_{3\times3} & \mathbf{0}_{3\times3} \\ \mathbf{0}_{3\times1} & (\boldsymbol{\omega}\times I')_{3\times3} \end{bmatrix}\dot{\boldsymbol{\chi}}$, $\bar{\mathbf{G}}(\boldsymbol{\chi}) = m\begin{bmatrix} \bar{\boldsymbol{g}} \\ \mathbf{0}_{3\times1} \end{bmatrix}$, $\dot{\boldsymbol{\chi}} = \begin{bmatrix} \dot{\mathbf{x}}_{\mathbf{p}} \\ \boldsymbol{\omega} \end{bmatrix}$, $\bar{\boldsymbol{g}} = \begin{bmatrix} 0 & 0 & -9.8 \end{bmatrix}^T$; m, $\mathbf{I}' = \mathbf{R}\mathbf{I}\mathbf{R}^T$, $\mathbf{x}_{\mathbf{p}} =$

$\left[\begin{array}{ccc} x & y & z \end{array}\right]^T$ and $\boldsymbol{\omega} = \left[\begin{array}{ccc} \omega_x & \omega_y & \omega_z \end{array}\right]^T$ are mass, the instantaneous inertia tensor of the moving platform relative to the inertial frame $[B]$, position and angular velocity of the end-effector.
$\bar{\boldsymbol{\tau}} = \left[\begin{array}{ccc} \mathbf{c_1} & \cdots & \mathbf{c_6} \\ (\mathbf{RP_{c1}}) \times \mathbf{c_1} & \cdots & (\mathbf{RP_{c6}}) \times \mathbf{c_6} \end{array}\right] \mathbf{f_c}$, and $\mathbf{c}_i$, $i = 1 \ldots 6$, is the unit vector along the prismatic linear actuators; $\boldsymbol{P_{ci}}$, $i = 1 \ldots 6$, is the vector from O_p to the connecting point of the actuators on the platform, $\boldsymbol{R}$ is the rotation matrix of the platform relative to the base, $\boldsymbol{f_c} = \left[\begin{array}{ccc} f_{c1} & \ldots & f_{c6} \end{array}\right]^T$ is the actuator force vector.

Property1: The matrix $\dot{\bar{\mathbf{D}}}(\boldsymbol{\chi}) - 2\bar{\mathbf{C}}(\boldsymbol{\chi}, \dot{\boldsymbol{\chi}})$ is a skew-symmetric matrix [14], i.e.

$$\mathbf{y}^T(\dot{\bar{\mathbf{D}}}(\boldsymbol{\chi}) - 2\bar{\mathbf{C}}(\boldsymbol{\chi}, \dot{\boldsymbol{\chi}}))\mathbf{y} = 0, \forall \mathbf{y} \in R^6. \tag{2}$$

The actual dynamics of the Parallel Robot including the structured and unstructured uncertainties is given by

$$\bar{\mathbf{D}}(\boldsymbol{\chi})\ddot{\boldsymbol{\chi}} + \bar{\mathbf{C}}(\boldsymbol{\chi}, \dot{\boldsymbol{\chi}})\dot{\boldsymbol{\chi}} + \bar{\mathbf{G}}(\boldsymbol{\chi}) = \boldsymbol{\tau} + \boldsymbol{\delta\tau}, \tag{3}$$

where $\boldsymbol{\delta\tau} = \mathbf{D_e}(\boldsymbol{\chi})\ddot{\boldsymbol{\chi}} + \mathbf{C_e}(\boldsymbol{\chi}, \dot{\boldsymbol{\chi}})\dot{\boldsymbol{\chi}} + \mathbf{G_e}(\boldsymbol{\chi})$, and $\mathbf{D_e}(\boldsymbol{\chi})$ and $\mathbf{C_e}(\boldsymbol{\chi}, \dot{\boldsymbol{\chi}})$ are modeling errors, and $\mathbf{G_e}(\boldsymbol{\chi})$ is the error of the gravitational torques.

With regard to the camera model, we assume that the projective geometry of the camera is modeled by perspective projection [9]. The camera uses the Frame E as the body frame and λ is the focal length of the camera lens. The $i-$th feature point $P_i = \left[\begin{array}{ccc} X_i & Y_i & Z_i \end{array}\right]^T$, in the camera frame E, will project onto the image plane with the coordinates $\left[\begin{array}{cc} x_i & y_i \end{array}\right]^T$, given by

$$\xi_i = \left[\begin{array}{c} x_i \\ y_i \end{array}\right] = -\alpha\frac{\lambda}{Z_i}\left[\begin{array}{c} X_i \\ Y_i \end{array}\right], \tag{4}$$

where ξ_i is the image feature point, α is the scaling factor, $|Z_i|$ is the distance from the camera to the object (depth) with $Z_i \leq 0$. Taking the time derivative on both sides of (4) we get

$$\dot{\xi}_i = -\alpha\frac{\lambda}{Z_i}\left[\begin{array}{ccc} 1 & 0 & -\frac{X_i}{Z_i} \\ 0 & 1 & -\frac{Y_i}{Z_i} \end{array}\right]\left[\begin{array}{c} \dot{X}_i \\ \dot{Y}_i \\ \dot{Z}_i \end{array}\right]. \tag{5}$$

According to [10], the following relationship holds

$$\begin{aligned} \left[\begin{array}{c} \dot{X}_i \\ \dot{Y}_i \\ \dot{Z}_i \end{array}\right] &= \omega_{be}^e \times p_i^e + v_{be}^e \\ &= \left[\begin{array}{cc} \mathbf{I}_{3\times3} & -p_i^e\times \end{array}\right]\left[\begin{array}{cc} R^T(\chi) & \mathbf{0}_{3\times3} \\ \mathbf{0}_{3\times3} & R^T(\chi) \end{array}\right]\left[\begin{array}{c} v_{be}^b \\ \omega_{be}^b \end{array}\right] \end{aligned} \tag{6}$$

where $\mathbf{I}_{3\times3}$ is identity matrix, $p_i^e\times$ denotes the skew symmetric cross product matrix of P_i, v_{be}^e and ω_{be}^e are the translation and angular velocity of the camera in E frame, v_{be}^b and ω_{be}^b are the camera translation and angular velocity with respect to the inertial frame B.

Finally substituting (6) into (5), we get the relationship between the image feature point velocity $\dot{\xi}_i$ and the camera translation and angular velocity v_{be}^b and ω_{be}^b

$$\dot{\xi}_i = J_{im}(\xi_i, Z_i)\left[\begin{array}{cc} R^T(\chi) & \mathbf{0}_{3\times3} \\ \mathbf{0}_{3\times3} & R^T(\chi) \end{array}\right]\left[\begin{array}{c} v_{be}^b \\ \omega_{be}^b \end{array}\right], \tag{7}$$

where J_{im} is the image Jacobian

$$J_{im}(\xi_i, Z_i) = \left[\begin{array}{cccccc} -\frac{\alpha\lambda}{Z_i} & 0 & -\frac{x_i}{Z_i} & \frac{x_i y_i}{\alpha\lambda} & -\frac{\alpha^2\lambda^2 + x_i^2}{\alpha\lambda} & -y_i \\ 0 & -\frac{\alpha\lambda}{Z_i} & -\frac{y_i}{Z_i} & \frac{\alpha^2\lambda^2 + y_i^2}{\alpha\lambda} & -\frac{x_i y_i}{\alpha\lambda} & x_i \end{array}\right] \tag{8}$$

In the above camera model, the position of the feature points of the object can be measured by the camera. The unknown parameter is depth Z_i. Let $Z_i = Zd_i + \Delta Z_i$ (Zd_i is the actual depth value and ΔZ_i is the measurement error) and substitute it into (8), we get the measured image Jacobian

$$\begin{aligned} &J_{m-im}(\xi_i, Z_i) = \\ &J_{r-im}(\xi_i, Zd_i) + J_{e-im}(\xi_i, Zd_i, \Delta Z_i), \end{aligned} \tag{9}$$

where $J_{r-im}(\xi_i, Zd_i) = J_{im}(\xi_i, Zd_i)$ is the real image Jacobian, and $J_{e-im}(\xi_i, Zd_i, \Delta Z_i)$ is the error image Jacobian.

For a static object with m feature points in the robot workspace, the image vector is defined as $\xi = \left[\begin{array}{ccc} \xi_1^T & \ldots & \xi_m^T \end{array}\right]^T$, and the measured image Jacobian is given by

$$J_{m-im}(\xi, Z) = J_{r-im}(\xi, Zd) + J_{e-im}(\xi, Zd, \Delta Z), \tag{10}$$

where $J_{r-im}(\xi, Zd) = \left[\begin{array}{c} J_{r-im}(\xi_1, Zd_1) \\ \vdots \\ J_{r-im}(\xi_m, Zd_m) \end{array}\right]$ and $J_{e-im}(\xi, Zd, \Delta Z) = \left[\begin{array}{c} J_{e-im}(\xi_1, Zd_1, \Delta Z_1) \\ \vdots \\ J_{e-im}(\xi_m, Zd_m, \Delta Z_m) \end{array}\right]$.

The relationship between the image feature point velocity $\dot{\xi}_i$ and the camera translation and angular velocity v_{be}^b and ω_{be}^b is the following:

$$\dot{\xi} = J_{m-im}(\xi, Z)\left[\begin{array}{cc} R^T(\chi) & \mathbf{0}_{3\times3} \\ \mathbf{0}_{3\times3} & R^T(\chi) \end{array}\right]\left[\begin{array}{c} v_{be}^b \\ \omega_{be}^b \end{array}\right]. \tag{11}$$

Because the camera use the E frame (which is also the body frame of the platform of the parallel robot) as the body frame, we have $v_{be}^b = \dot{x}_p$, and $\omega_{be}^b = \omega$. Let $K(\chi) = \left[\begin{array}{cc} R^T(\chi) & \mathbf{0}_{3\times3} \\ \mathbf{0}_{3\times3} & R^T(\chi) \end{array}\right]$, $J = J_{r-im}(\xi, Zd)K(\chi)$ and $\Delta J = J_{e-im}(\xi, Zd, \Delta Z)K(\chi)$, (11) becomes

$$\dot{\xi} = (J + \Delta J)\dot{\chi}. \tag{12}$$

III. The adaptive supervisory fuzzy logic controller and the Hybrid Controller

Because the fuzzy systems can approximate any real continuous function to arbitrary accuracy [11], an ASFLC consisting of six parallel connected fuzzy logic systems (FLS) is first designed to compensate the uncertainties. The singleton fuzzifier, the product-operation rule of fuzzy implication, center of average deffuzifier and bell membership functions are implemented for each FLS. The final output of each FLS is the weighted average of all rule outputs, computed as follows:

$$\tau_{fj} = \sum_{i=1}^{M} \omega_f^i \bar{\phi}_f^i = \frac{\omega_f^1 \phi_f^1 + \ldots + \omega_f^M \phi_f^M}{\phi_f^1 + \ldots + \phi_f^M} = \boldsymbol{\omega}_f^T \bar{\boldsymbol{\phi}}_f, \quad (13)$$

where $\boldsymbol{\omega}_f = \begin{bmatrix} \omega_f^1 & \ldots & \omega_f^M \end{bmatrix}^T$ is the parameter vector. Each ω_f^i is the point at which the output function reaches its maximal value and $\bar{\boldsymbol{\phi}}_f = \begin{bmatrix} \bar{\phi}_f^1 & \ldots & \bar{\phi}_f^M \end{bmatrix}^T$ is the function basis vector. The vector $\boldsymbol{\omega}_f$ will be adjusted by an adaptive algorithm which thereby determines stabilizing membership functions.

The input linguistic vector to the ASFLC is $\boldsymbol{\chi}_f = \begin{bmatrix} \tilde{\xi}^T & \dot{\tilde{\xi}}^T \end{bmatrix}^T$, and the output linguistic variable is $\boldsymbol{\tau_f}$. $\tilde{\xi}$ is the image feature error defined as $\tilde{\xi} = \xi_d - \xi$, ξ_d is the desired image feature vector, and ξ is the actual image feature vector. The input linguistic variables of the ASFLC defined on the normalized universe of discourse [-1,1] include seven linguistic terms: PB, PM, PS, ZE, NS, NM and NB. The rule-base including $M = 49$ IF-THEN rules for each FLS is listed in the table shown in (a) of Fig. (2).

Before the derivation of the hybrid controller, the following assumptions are made:
1)The initial feature error $\tilde{\xi}(0)$ is sufficiently small [12].
2)The feature points (that can avoid local minima and task singularity) on a static object are given.

Remark1: Redundant image points ($m = 4$) are considered in order to guarantee the image Jacobian is full-rank.

Theorem 3.1: If the parallel robot has the dynamics in the form of (3), the camera model is in the form of (12), the control law is chosen as the following:

$$\boldsymbol{\tau} = \tau_{im} - \tau_f, \quad (14)$$

where $\boldsymbol{\tau}_f = [\tau_{f1} \ldots \tau_{f6}]^T$ is the output of the ASFLC, τ_{im} is the output of the image-based controller (IBC) in the following form:

$$\tau_{im} = J^T K_p^T \tilde{\xi} - K_v sgn(\dot{\chi}) + \bar{\mathbf{G}}(\boldsymbol{\chi}), \quad (15)$$

where $J = J_{r-im}(\xi, Zd)K(\chi)$, $K_p = diag\,(k_{p1}, \ldots, k_{p8})$ and $K_v = diag\,(k_{v1}, \ldots, k_{v8})$, with $k_{pi} > 0$, $k_{vi} > 0$, $i = 0, \ldots, 8$. The adaptive law of the ASFLC is chosen as (22), and the minimum approximation error is $\boldsymbol{\gamma} = [\gamma_1 \ldots \gamma_6]^T = \Delta\boldsymbol{\tau} - \boldsymbol{\tau_f^*}$, $max|\gamma_i| \leq \eta_\Delta$ and $k_{vi} \geq \eta_\Delta + \eta_i$, then the system is Lyapunov stable.

Proof. Considering the following Lyapunov function candidate:

$$V = \frac{1}{2}\dot{\boldsymbol{\chi}}^T \bar{\mathbf{D}} \dot{\boldsymbol{\chi}} + \frac{1}{2}\tilde{\xi}^T K_p \tilde{\xi} + \frac{1}{2}\sum_{i=1}^{6} \tilde{\omega}_{fi}^T \Psi_i \tilde{\omega}_{fi}, \quad (16)$$

where Ψ_i, $i = 1 \ldots 6$, is a positive real constant, $\tilde{\omega}_{fi}$ is the error between the optimal parameters and the actual parameters. Taking the first time derivative of (16), and using (3), we have

$$\begin{aligned} \dot{V} &= \dot{\boldsymbol{\chi}}^T \bar{\mathbf{D}} \ddot{\boldsymbol{\chi}} + \frac{1}{2}\dot{\boldsymbol{\chi}}^T \dot{\bar{\mathbf{D}}} \dot{\boldsymbol{\chi}} + \dot{\tilde{\xi}}^T K_p \dot{\tilde{\xi}} + \sum_{i=1}^{6} \tilde{\omega}_{fi}^T \Psi_i \dot{\tilde{\omega}}_{fi} \\ &= \dot{\boldsymbol{\chi}}^T (\boldsymbol{\tau} + \boldsymbol{\delta\tau} - \bar{\mathbf{C}}\dot{\boldsymbol{\chi}} - \bar{\mathbf{G}}(\boldsymbol{\chi}) + \frac{1}{2}\dot{\bar{\mathbf{D}}}\dot{\boldsymbol{\chi}}) + \dot{\tilde{\xi}}^T K_p \dot{\tilde{\xi}} \\ &\quad + \sum_{i=1}^{6} \tilde{\omega}_{fi}^T \Psi_i \dot{\tilde{\omega}}_{fi}. \end{aligned} \quad (17)$$

Using Property 1 and substituting (12) into (17), with $\dot{\xi}_d = 0$, we have

$$\begin{aligned} \dot{V} &= \dot{\boldsymbol{\chi}}^T (\boldsymbol{\tau} + \boldsymbol{\delta\tau} - \bar{\mathbf{G}}(\boldsymbol{\chi}) - \mathbf{J}^T K_p^T \tilde{\xi} - \Delta J^T K_p^T \tilde{\xi}) \\ &\quad + \sum_{i=1}^{6} \tilde{\omega}_{fi}^T \Psi_i \dot{\tilde{\omega}}_{fi}. \end{aligned} \quad (18)$$

Letting $\boldsymbol{\Delta\tau} = [\Delta\tau_1 \ldots \Delta\tau_6]^T = \boldsymbol{\delta\tau} - \Delta J^T K_p^T \tilde{\xi}$ be the overall uncertainty of the system, then (18) becomes

$$\dot{V} = \dot{\boldsymbol{\chi}}^T (\boldsymbol{\tau} + \boldsymbol{\Delta\tau} - \bar{\mathbf{G}} - \mathbf{J}^T K_p^T \tilde{\xi}) + \sum_{i=1}^{6} \tilde{\omega}_{fi}^T \Psi_i \dot{\tilde{\omega}}_{fi}. \quad (19)$$

Let $\boldsymbol{\tau_f} = [\tau_{f1} \ldots \tau_{f6}]^T$ be the output of the ASFLC, which is used to approximate $\boldsymbol{\Delta\tau}$, let the optimal approximation of $\boldsymbol{\Delta\tau}$ be $\boldsymbol{\tau_f^*} = \begin{bmatrix} \tau_{f1}^* \ldots \tau_{f6}^* \end{bmatrix}^T$, then $\tau_{fi} = \boldsymbol{\omega_{fi}}^T \bar{\boldsymbol{\phi}}_{\boldsymbol{fi}}$, and $\tau_{fi}^* = \boldsymbol{\omega_{fi}^*}^T \bar{\boldsymbol{\phi}}_{\boldsymbol{fi}}$, $i = 1 \ldots 6$. Define the error between the optimal parameters and the actual parameters as $\tilde{\boldsymbol{\omega}}_{\boldsymbol{f}} = [\tilde{\boldsymbol{\omega}}_{\boldsymbol{f1}} \ldots \tilde{\boldsymbol{\omega}}_{\boldsymbol{f6}}]^T$, and $\tilde{\boldsymbol{\omega}}_{\boldsymbol{fi}} = \boldsymbol{\omega_{fi}^*} - \boldsymbol{\omega_{fi}}$, $i = 1 \ldots 6$, then $\boldsymbol{\tau_f^*} - \boldsymbol{\tau_f} = \begin{bmatrix} \tilde{\boldsymbol{\omega}}_{\boldsymbol{f1}}^T \bar{\boldsymbol{\phi}}_{\boldsymbol{f1}} \ldots \tilde{\boldsymbol{\omega}}_{\boldsymbol{f6}}^T \bar{\boldsymbol{\phi}}_{\boldsymbol{f6}} \end{bmatrix}^T$.

Choosing the control as (14), and substituting it into (19), we have

$$\begin{aligned} \dot{V} &= \dot{\boldsymbol{\chi}}^T (\boldsymbol{\Delta\tau} - \boldsymbol{\tau_f} - K_v sgn(\dot{\chi})) + \sum_{i=1}^{6} \tilde{\omega}_{fi}^T \Psi_i \dot{\tilde{\omega}}_{fi} \\ &= \dot{\boldsymbol{\chi}}^T (\boldsymbol{\Delta\tau} - \boldsymbol{\tau_f^*} + \boldsymbol{\tau_f^*} - \boldsymbol{\tau_f} - K_v sgn(\dot{\chi})) \\ &\quad + \sum_{i=1}^{6} \tilde{\omega}_{fi}^T \Psi_i \dot{\tilde{\omega}}_{fi}. \end{aligned} \quad (20)$$

Finally, letting the minimum approximation error be $\boldsymbol{\gamma} =$

$\dot{\tilde{\xi}}$ \ $\tilde{\xi}$	NB	NM	NS	ZE	PS	PM	PB
NB	PB	PB	PB	PB	PM	PS	ZE
NM	PB	PB	PB	PM	PS	ZE	NS
NS	PB	PB	PM	PS	ZE	NS	NM
ZE	PB	PM	PS	ZE	NS	NM	NB
PS	PM	PS	ZE	NS	NM	NB	NB
PM	PS	ZE	NS	NM	NB	NB	NB
PB	ZE	NS	NM	NB	NB	NB	NB

(a)

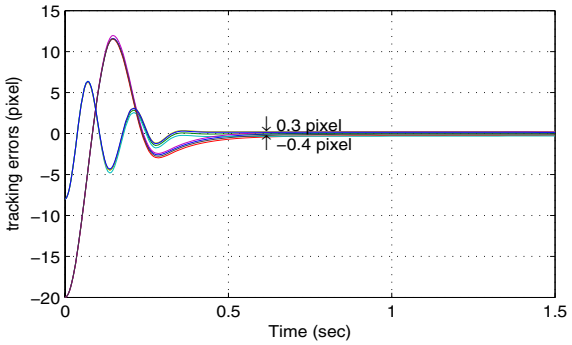

(b)

Fig. 2. Fuzzy rule table and tracking errors

$[\gamma_1 \dots \gamma_6]^T = \Delta\boldsymbol{\tau} - \boldsymbol{\tau}_{\boldsymbol{f}}^*$, we have

$$\begin{aligned}\dot{V} &= \dot{\boldsymbol{\chi}}^T(\boldsymbol{\gamma} - K_v sgn(\dot{\chi})) + \dot{\boldsymbol{\chi}}^T(\boldsymbol{\tau}_{\boldsymbol{f}}^* - \boldsymbol{\tau}_{\boldsymbol{f}}) \\ &\quad + \sum_{i=1}^{6} \tilde{\omega}_{fi}^T \Psi_i \dot{\tilde{\omega}}_{fi} \\ &= \dot{\boldsymbol{\chi}}^T(\boldsymbol{\gamma} - K_v sgn(\dot{\chi})) + \sum_{i=1}^{6} \tilde{\boldsymbol{\omega}}_{\boldsymbol{fi}}^{\boldsymbol{T}}(\dot{\boldsymbol{\chi}}_{\boldsymbol{i}} \bar{\boldsymbol{\phi}}_{\boldsymbol{fi}} + \Psi_i \dot{\tilde{\omega}}_{fi}) \\ &. \end{aligned} \tag{21}$$

Choose $\dot{\boldsymbol{\chi}}_{\boldsymbol{i}} \bar{\boldsymbol{\phi}}_{\boldsymbol{fi}} + \Psi_i \dot{\tilde{\omega}}_{fi} = 0$, we have

$$\dot{\boldsymbol{\chi}}_{\boldsymbol{i}} \bar{\boldsymbol{\phi}}_{\boldsymbol{fi}} = -\Psi_i \dot{\tilde{\omega}}_{fi} = \Psi_i \dot{\omega}_{fi}. \tag{22}$$

Note that $\dot{\boldsymbol{\chi}}$ is known from the robot's joint velocity measurements, transformed to task space.

Substituting (22) into (21), we have

$$\begin{aligned}\dot{V} &= \dot{\boldsymbol{\chi}}^T(\boldsymbol{\gamma} - K_v sgn(\dot{\chi})) \\ &\leq \sum_{i=1}^{6}(|\dot{\chi}_i|\gamma_i - k_{vi}|\dot{\chi}_i|) \\ &= \sum_{i=1}^{6}(\gamma_i - k_{vi})|\dot{\chi}_i|. \end{aligned} \tag{23}$$

Let $max|\gamma_i| \leq \eta_\Delta$, if $k_{vi} \geq \eta_\Delta + \eta_i$, $\eta_i \geq 0$ (is a constant), then we have

$$\dot{V} \leq -\sum_{i=1}^{6} \eta_i |\dot{\chi}_i| \leq 0. \tag{24}$$

From (16) and (24), we know that the Lyapunov function candidate is positive definite and the derivative of the Lyapunov function is negative semidefinite, so according to the Lyapunov stability theorem [13], the system is stable in the Lyapunov sense.

IV. Simulation

In this section, simulation of the set-point regulation for a micro parallel robot is done to verify the effectiveness of the proposed controller. The parallel robot is shown as in Fig. (1). The maximal modeling error $\mathbf{C_e}$ is $\pm 12.5\%$ of the estimated value $\bar{\mathbf{C}}$, $|\mathbf{C_e}| \leq 0.125|\bar{\mathbf{C}}|$, and the maximal modeling error $\mathbf{D_e}$ is $\pm 7.5\%$ of the estimated value $\bar{\mathbf{D}}$, $|\mathbf{D_e}| \leq 0.075|\bar{\mathbf{D}}|$. $|\mathbf{Pc_i}| = 0.1(m)$, $i = 1 \dots 6$, is the length from Op to the connecting point of the actuators on the platform, $|\mathbf{Bc_i}| = 0.2(m)$, $i = 1 \dots 6$, is the length from Ob to the connecting point of the actuators on the base. The mass of the platform is $m = 0.06(kg)$. A camera with the focal length $\lambda = 0.008(m)$ is used in the simulation. For the sake of simplicity, we use an average value as the scale factor α, and $\alpha = 72727(pixels/m)$. To guarantee full-rank of the image matrix, achieve robust visual position regulation and eliminate bad features, redundant image points (four image points) are used in the simulation. The maximal measurement error of the object depth is $\Delta Zi = 0.3Zdi$. The initial image feature points are $\xi(0) = \begin{bmatrix} 30 & 18 & 65 & -65 & -44 & 37 & -10 & -15 \end{bmatrix}^T$, the desired image feature points are $\xi_d = \begin{bmatrix} 10 & 10 & 45 & -73 & -64 & 29 & -30 & -23 \end{bmatrix}^T$.

The simulation results are shown in Fig. (2∼5). From (b) of Fig. (2), we can see that the feature position errors of the four features points are in a small neighborhood of zero. Fig. (3) depicts the position trajectory of the image feature points from $\xi(0)$ to ξ_d, which shows that the feature points converge to the desired positions. The trajectories of the platform are shown in Fig. (4), which shows that at the end of the simulation, the platform is static in the final position. Fig. (5) shows that only a small control effort is needed for the position regulation.

V. Conclusion

In this paper, a new type of parallel robot based precision pointing systems (PRBPPS) is put forward. By combining the excellent disturbance rejection ability of the parallel robot, the performance of the precision pointing systems can be increased. The dynamics of the parallel robots with parameter uncertainties is combined into the controller design. The uncertainties of the parallel robots and the uncertainties of the object depth are compensated by the adaptive supervisory fuzzy logic controller (ASFLC). A hybrid controller including the image-based nonlinear controller and ASFLC

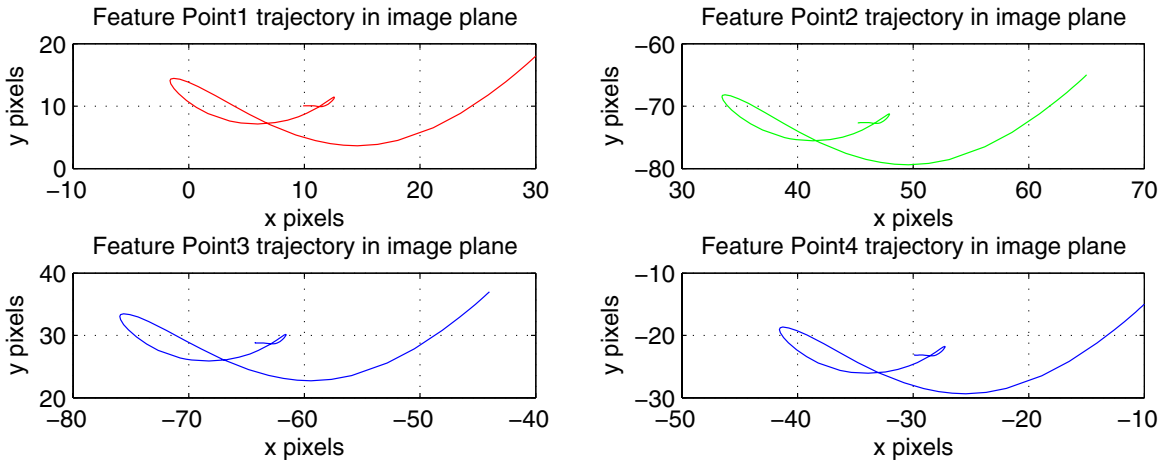

Fig. 3. Feature position trajectory in the image plane

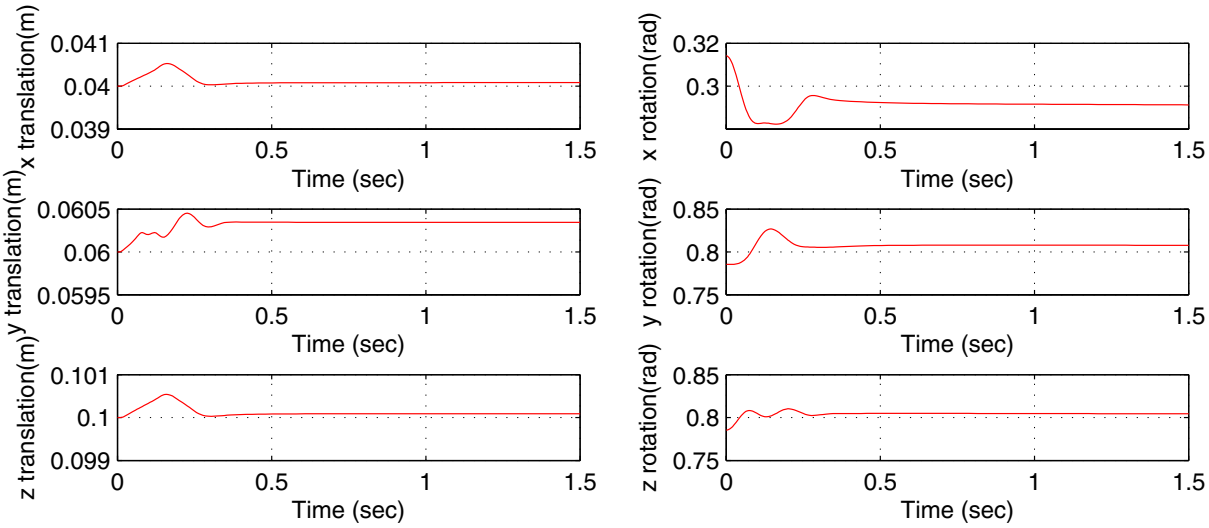

Fig. 4. The trajectory of the platform.

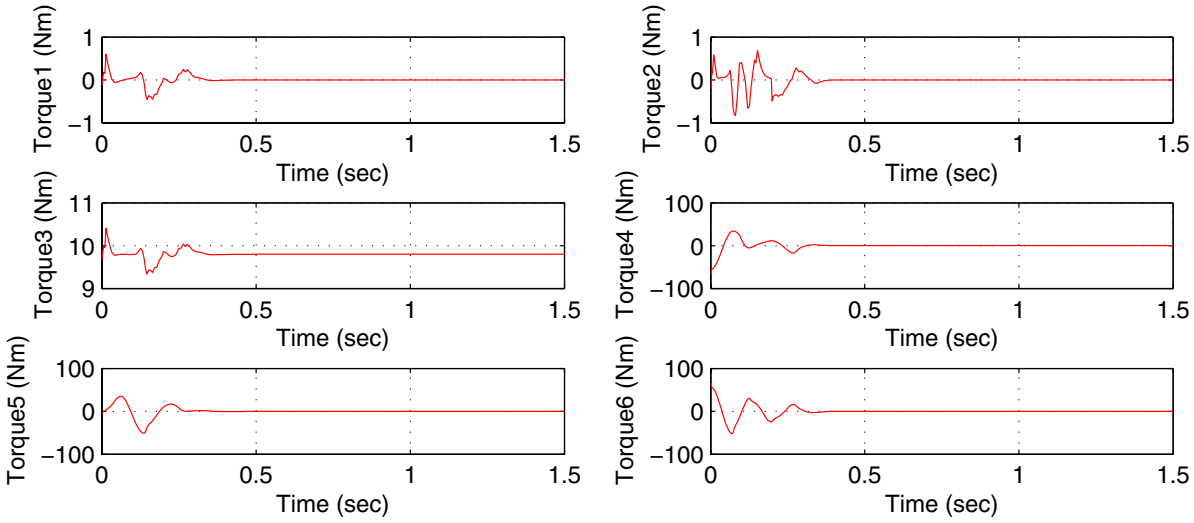

Fig. 5. The control torque of the parallel robot.

is derived by using the Lyapunov direct method to realize the precision position regulation (PPR). The simulation results shows that the PRBPPS realizes PPR with very good robustness to the parameter uncertainties.

REFERENCES

[1] Robert Mahony, Tarek Hamel, Francois Chaumette. A Decoupled Image Space Approach to Visual Servo Control of a Robotic Manipulator. Proceedings of the 2002 IEEE International Conference on Robotics and Automation, Washington, DC, pp. 3781-3786, May, 2002.

[2] F. Chaumette, Ezio Malis. 2 1/2 D visual servoing: a possible solution to improve image-based and position-based visual servoings. IEEE Int. Conf. on Robotics and Automation, ICRA 2000, San Francisco, Carifornia, Apri 2000.

[3] Seth Hutchinson, Gregory D. Hager, and Peter I. Corke. A Tutorial on Visual Servo Control. IEEE Transactions on Robotics and Automation, Vol. 12, NO. 5, pp. 651-670 Oct 1996.

[4] J. E. McInroy, J. F. OBrien, and G. W. Neat. Precise, fault tolerant pointing using a Stewart platform. IEEE/ASME Trans. Mechatron, vol. 4, pp. 91-95, Mar. 1999.

[5] J. E. McInroy and J. C. Hamann. Design and control of flexure jointed hexapods. IEEE Trans. Robot. Automat., vol. 16, pp. 372-381, Aug. 2000.

[6] Haomin Lin and John E. McInroy. Adaptive Sinusoidal Disturbance Cancellation for Precise Pointing of Stewart Platforms. IEEE Trans. Control Syst. Technology, vol. 11, no. 2, MARCH 2003.

[7] Z. Geng and L. S. Haynes. Six degree-of-freedom active vibration isolation using Stewart platform manipulator. J. Robot. Syst., vol. 10, no. 5, pp. 725-744, 1993.

[8] L Vaillon, B Petitjean, B Frapard and D Lebihan. Active isolation in space truss structures: from concept to implementation. Smart Material and Structures, 8(1999), pp. 781-790.

[9] B. K. P. Horn, Robot Vision. Cambridge, MA: MIT Press, 1986.

[10] Richard M. Murray, Zexiang Li, and S. Shankar Sastry. A Mathematical Introduction to Robotic Manipulation. CRC, March 22, 1994.

[11] L.X. Wang. Adaptive Fuzzy Systems and Control. Englewood liffs,NJ:Printice-Hall,1994.

[12] Rafael Kelly, Member, IEEE, Ricardo Carelli, Senior Member, IEEE, Oscar Nasisi, Benjam Kuchen, Member, IEEE, and Fernando Reyes. Stable Visual Servoing of Camera-in-Hand robotic Systems. IEEE/ASME TRANSACTIONS ON MECHATRONICS, VOL. 5, NO. 1, pp. 39-48, MARCH 2000.

[13] J. Slotine and W. Li. Applied Nonlinear Control. Englewood Cliffs, NJ: Prentice-Hall, 1991.

[14] Zhen Qi, John E. McInroy, Farhad Jafari. Trajectory Tracking with Parallel Robots Using Low Chattering, Fuzzy Sliding Mode Controller. Journal of Intelligent and Robotic Systems. December 08, 2006.